Available online at www.sciencedirect.com
SCIENCE DIRECT®
ELSEVIER
European Journal of Mechanics B/Fluids 22 (2003) 473–486

Forced convection past a heated cylinder in a porous medium using a thermal nonequilibrium model: boundary layer analysis

D. Andrew S. Rees [a,*], Andrew P. Bassom [b,c], Ioan Pop [d]

[a] *Department of Mechanical Engineering, University of Bath, Claverton Down, Bath, BA2 7AY, UK*
[b] *School of Mathematical Sciences, University of Exeter, North Park Road, Exeter EX4 4QE, Devon, UK*
[c] *School of Mathematics, University of New South Wales, Sydney, 2052, Australia*
[d] *Faculty of Mathematics, University of Cluj, R-3400 Cluj, CP253, Romania*

Received 18 March 2003; received in revised form 27 May 2003; accepted 23 June 2003

Abstract

We study the forced convective heat transfer from a uniform temperature cylinder placed perpendicular to an otherwise uniform fluid stream in a porous medium. Attention is focussed on how the absence of local thermal equilibrium between the solid and fluid phases affects the rate of heat transfer from the cylinder when the Péclet number is very large. It is found in all cases that the surface rate of heat transfer for the fluid is always greater than that of the solid matrix. Detailed numerical results are given for a wide range of parameter values, and these are supplemented by asymptotic analyses for both small and large values of the inter-phase heat transfer coefficient, H. When this coefficient is small the thermal field corresponding to the solid phase occupies a much greater region than does the thermal field of the fluid phase.

Keywords: Forced convection; Porous media; Cylinder; Boundary layer; Local thermal nonequilibrium

1. Introduction

It is well accepted that the topic of convective flow in porous media is of major importance in many natural and practical situations. Technological applications include geothermal energy systems, prevention of subsoil water pollution, thermal insulation systems, heat exhangers and nuclear waste repositories, to name but a few. In recent times porous medium models have also been applied in simulating more generalised situations such as flow through packed beds, liquid metal flow through dendritic structures in alloy casting and even for obtaining approximate solutions for flow through turbomachinery. Reviews of the huge volume of information on this subject can be found in the recent books by Ingham and Pop [1], Nield and Bejan [2] and Vafai [3]. Despite the great quantity of work addressing various problems in porous media, there is still a need for comprehensive and reliable methods of predicting accurately the flow and heat transfer characteristics in many cases. The inclusion of more physical realism in the governing Darcian fluid models is important for the accurate modeling of practical problems.

Most of the analytical and numerical studies of flow and heat transfer in porous media assume the condition of local thermal equilibrium (LTE) between the solid and the fluid materials. By this is meant that the solid and fluid phases are taken to have the same temperature locally over length scales which are small compared with the macroscopic environment, but large compared with the detailed microstructure of the medium. However, in applications using porous media, such as chemical reactors, thermal energy transport/storage systems and cooling of electronic devices, a temperature discrepancy between the solid matrix and the

* Corresponding author.
E-mail address: d.a.s.rees@bath.ac.uk (D.A.S. Rees).

0997-7546/$ – see front matter
doi:10.1016/S0997-7546(03)00055-4

saturating fluid has been observed and recognized. Correspondingly, an analysis of separate energy equations for the fluid and the solid, that is, a local nonequilibrium model, has assumed an increasing importance.

Nield and Kuznetsov [4] have shown that there are several industrial applications where high speed flow in a saturated porous medium leads to a significant degree of local thermal nonequilibrium. Examples of where this model applies are fixed bed nuclear propulsion systems and nuclear reactor modelling where the temperature difference between the liquid coolant and the solid rods is of great importance. A third example incorporates the storage of thermal energy derived from a solar energy conversion system, where a heated fluid flows from the solar collectors into a bed rock, and energy is recovered by reversing the flow in the bed. Other examples mentioned by Nield and Kuznetsov [4] and, more recently, by Nield et al. [5], include storage systems which have been designed for space power supply systems, where phase change material is used to enhance the efficiency, and the use of highly porous media (Brinkman model) in the cooling of electronic equipments.

The first studies of the convective flow through a porous medium when the fluid and the medium are not in LTE were concerned with free convection. Combarnous [6] and Combarnous and Bories [7] investigated the Darcy–Bénard problem using a two-temperature model. An extension of this system to forced convection flow through a porous packed bed has been undertaken by Sözen and Vafai [8], Sözen et al. [9], Amiri and Vafai [10] and Kuznetsov [11–13]. Interest in the two-temperature model has increased in the last few years and detailed reviews of other research have recently been given by Kuznetsov [14] and Vafai and Amiri [15].

Nield and Bejan [2] present the basic equations which are taken to account for the use of a nonequilibrium model of microscopic heat transfer between the fluid and the solid phase of the porous medium, but little work has been devoted to the study of external convective flow. The most recent studies of free convection over vertical surfaces and near the stagnation point of a cylinder surface embedded in a porous medium have been carried out by Rees and Pop [16,17] and Rees [18].

In this paper we study forced convection flow past a heated horizontal circular cylinder which is embedded in a porous medium and adopt the two-temperature model of microscopic heat transfer. Forced convection flow past a horizontal cylinder placed in a viscous (non-porous) or in a porous medium is probably one of the most extensively studied problem in fluid mechanics owing to its practical significance. In fact, the present work extends that of Pop and Yan [19] to account for the absence of local thermal equilibrium between the fluid and solid phases. (In passing it should be noted that Sano [20] has investigated unsteady forced convection flow past a horizontal circular cylinder but that work did not incorporate the the two-temperature flow model.)

Our problem is formulated in Section 2 while in Section 3 it is shown that at high values of the Péclet number, for which the boundary-layer approximation is valid, the governing Darcy and energy equations reduce to a parabolic partial differential system. Numerical solutions using the standard Keller box method are presented in Section 4 and these are followed by asymptotic analyses for large and small values of the microscopic solid/fluid heat transfer parameter, H, in Sections 5 and 6. A brief discussion closes the paper.

2. Formulation of the problem

We consider the forced convection flow past a heated horizontal circular cylinder of radius, a, which is embedded in a porous medium. We assume that the free stream velocity is U and that the temperatures of the cylinder and of the ambient fluid are T_c and T_∞, respectively, where $T_c > T_\infty$. Of prime concern in the present work is to determine how the heat transfer characteristics of this system are altered when the fluid and solid matrix comprising the porous medium are not in local thermal equilibrium. The governing steady two-dimensional equations for forced convection flow may be written

$$\frac{\partial(\bar{r}\,\bar{u})}{\partial \bar{r}} + \frac{\partial \bar{v}}{\partial \alpha} = 0, \tag{1a}$$

$$\bar{u} = -\frac{K}{\mu}\frac{\partial \bar{p}}{\partial \bar{r}}, \qquad \bar{v} = -\frac{K}{\mu}\frac{1}{\bar{r}}\frac{\partial \bar{p}}{\partial \alpha}, \tag{1b,c}$$

$$\varepsilon k_f\left(\frac{\partial^2 T_f}{\partial \bar{r}^2} + \frac{1}{\bar{r}}\frac{\partial T_f}{\partial \bar{r}} + \frac{1}{\bar{r}^2}\frac{\partial^2 T_f}{\partial \alpha^2}\right) = (\rho c)_f\left(\bar{u}\frac{\partial T_f}{\partial \bar{r}} + \frac{\bar{v}}{\bar{r}}\frac{\partial T_f}{\partial \alpha}\right) + h(T_f - T_s), \tag{1d}$$

$$(1-\varepsilon)k_s\left(\frac{\partial^2 T_s}{\partial \bar{r}^2} + \frac{1}{\bar{r}}\frac{\partial T_s}{\partial \bar{r}} + \frac{1}{\bar{r}^2}\frac{\partial^2 T_s}{\partial \alpha^2}\right) = h(T_s - T_f); \tag{1e}$$

see Nield and Bejan [2]. Here $\bar{u}$ and $\bar{v}$ denote the fluid seepage velocities in the radial and tangential directions, $\bar{r}$ and α, respectively. The pressure is $\bar{p}$, the temperature T and the other fluid and porous medium properties are the permeability K, the fluid viscosity μ, conductivity k, density ρ, specific heat c and the porosity ϵ. The subscripts f and s denote fluid and solid, respectively. Of especial interest is the coefficient, h, which is used to model the microscopic transfer of heat between the fluid

and solid phases. The value of h depends not only on the nature of the porous medium and the saturating fluid, but also on the microscopic Reynolds number; see Kuznetsov [14] and papers cited therein.

Eqs. (1) may be nondimensionalised using the transformations

$$\bar{r} = ar, \qquad (\bar{u}, \bar{v}) = U(u, v), \tag{2a,b}$$

$$T_f = (T_c - T_\infty)\theta + T_\infty, \qquad T_s = (T_c - T_\infty)\phi + T_\infty, \tag{2c,d}$$

and further simplification is afforded by the introduction of a streamfunction, ψ, according to

$$u = \frac{1}{r}\frac{\partial \psi}{\partial \alpha} \quad \text{and} \quad v = -\frac{\partial \psi}{\partial r}. \tag{2e,f}$$

After these transformations, Eqs. (1) become

$$\frac{\partial^2 \psi}{\partial r^2} + \frac{1}{r}\frac{\partial \psi}{\partial r} + \frac{1}{r^2}\frac{\partial^2 \psi}{\partial \alpha^2} = 0, \tag{3a}$$

$$\frac{1}{Pe}\left[\frac{\partial^2 \theta}{\partial r^2} + \frac{1}{r}\frac{\partial \theta}{\partial r} + \frac{1}{r^2}\frac{\partial^2 \theta}{\partial \alpha^2}\right] = \frac{1}{r}\left[\frac{\partial \psi}{\partial \alpha}\frac{\partial \theta}{\partial r} - \frac{\partial \psi}{\partial r}\frac{\partial \theta}{\partial \alpha}\right] + H(\theta - \phi), \tag{3b}$$

$$\frac{1}{Pe}\left[\frac{\partial^2 \phi}{\partial r^2} + \frac{1}{r}\frac{\partial \phi}{\partial r} + \frac{1}{r^2}\frac{\partial^2 \phi}{\partial \alpha^2}\right] = H\gamma(\phi - \theta), \tag{3c}$$

where

$$H = \frac{ah}{U(\rho c)_f}, \quad \gamma = \frac{\varepsilon k_f}{(1-\varepsilon)k_s} \quad \text{and} \quad Pe = \frac{Ua(\rho c)_f}{\varepsilon k_f} \tag{4a,b,c}$$

are dimensionless constants. Eqs. (3) need to be solved subject to the boundary conditions

$$\psi = 0, \quad \theta = \phi = 1 \quad \text{on} \quad r = 1 \quad \text{and} \quad \psi \to r\sin\alpha, \quad \theta, \phi \to 0 \quad \text{as} \quad r \to \infty. \tag{5}$$

In Eq. (4), H represents the dimensionless inter-phase heat transfer coefficient and γ is a porosity-scaled conductivity ratio, which we will allow to take values in the range from 10^{-2} to 10^2, which covers most practical applications. Low values of γ generally correspond to a relatively poorly conducting fluid such as air in a metallic porous medium. Lastly, the value Pe is a Péclet number based on the fluid properties and scaled with the porosity.

3. Boundary layer analysis

We shall consider forced convection at high values of the Péclet number and within this regime the heat transfer problem reduces to boundary-layer type – otherwise fully elliptic equations must be solved (see Wong et al. [21] for further details). The flow past the cylinder is given by the solution of Eq. (3a) and is, simply,

$$\psi = \left(r - \frac{1}{r}\right)\sin\alpha; \tag{6}$$

which returns to a uniform free stream when r is large. On substitution into (3b,c) we obtain equations for the temperature fields;

$$\frac{1}{Pe}\left[\frac{\partial^2 \theta}{\partial r^2} + \frac{1}{r}\frac{\partial \theta}{\partial r} + \frac{1}{r^2}\frac{\partial^2 \theta}{\partial \alpha^2}\right] = \left(1 - \frac{1}{r^2}\right)\cos\alpha\,\frac{\partial \theta}{\partial r} - \left(\frac{1}{r} + \frac{1}{r^3}\right)\sin\alpha\,\frac{\partial \theta}{\partial \alpha} + H(\theta - \phi), \tag{7a}$$

$$\frac{1}{Pe}\left[\frac{\partial^2 \phi}{\partial r^2} + \frac{1}{r}\frac{\partial \phi}{\partial r} + \frac{1}{r^2}\frac{\partial^2 \phi}{\partial \alpha^2}\right] = H\gamma(\phi - \theta). \tag{7b}$$

When the fluid and solid matrix are in local thermal equilibrium Pop and Yan [19] showed that the thermal field is contained within a boundary layer which is thin compared with the radius of the cylinder whenever Pe is large. This remains the case when LTE no longer applies. That this is so may be seen in Fig. 1 which shows the temperature fields for $Pe = 100$, $H = 0.3$ and $\gamma = 1$ which were computed by solving Eqs. (7); see Wong et al. [21] for further cases. In this figure we see that the thermal boundary layer thickens with distance from the upstream (front) stagnation point. Also visible is the difference in the boundary layer thickness between the fluid and solid phases. Following [19], then, we rescale the radial coordinate according to

$$r = 1 + Pe^{-1/2}\hat{r}, \tag{8}$$

whereupon (7a,b) take the forms

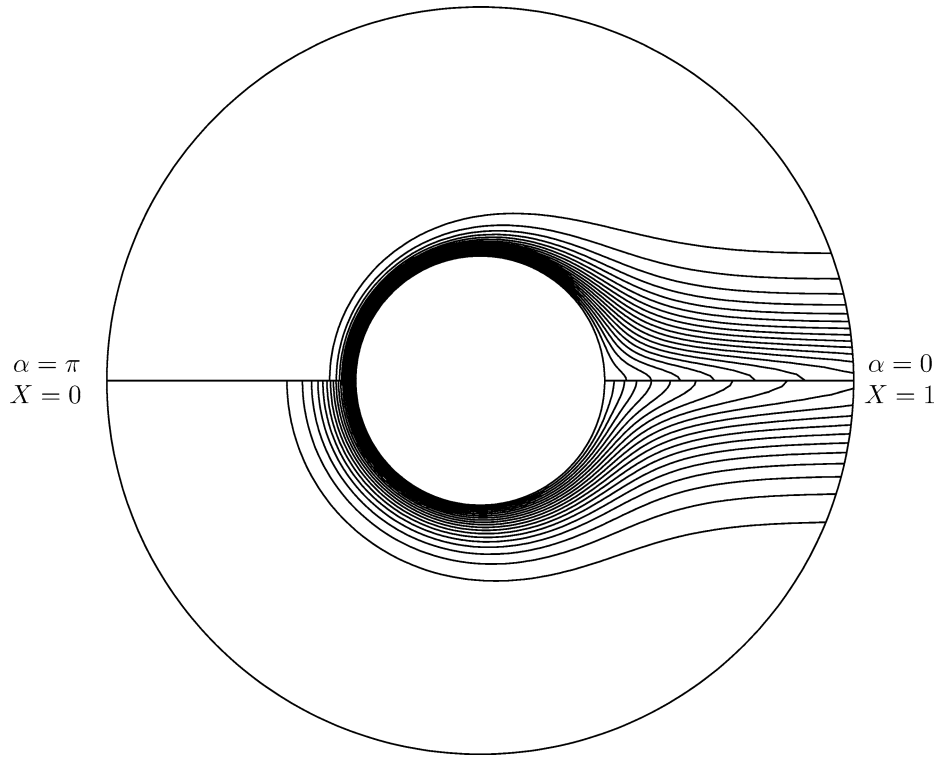

Fig. 1. Computation of the temperature field for forced convection flow past a cylinder in a porous medium for $Pe = 100$, $H = 0.3$ and $\gamma = 1$. Fluid flows from left to right. The upstream (front) stagnation point corresponds to both $\alpha = \pi$ and $X = 0$. The upper half shows isotherms for the fluid phase, while the lower half corresponds to the solid phase. Isotherms are drawn at intervals of 0.05.

$$\frac{\partial^2\theta}{\partial\hat{r}^2} = 2\hat{r}\cos\alpha\frac{\partial\theta}{\partial\hat{r}} - 2\sin\alpha\frac{\partial\theta}{\partial\alpha} + H(\theta-\phi), \tag{9a}$$

$$\frac{\partial^2\phi}{\partial\hat{r}^2} = H\gamma(\phi-\theta), \tag{9b}$$

at leading order in *Pe*. Given the form of the similarity solutions presented in [19] for the LTE case, we introduce the transformations

$$\eta = \hat{r}\sin\tfrac{1}{2}\alpha \quad \text{and} \quad X = \cos\tfrac{1}{2}\alpha, \tag{10}$$

noting that $X = 0$ corresponds to the upstream stagnation point on the cylinder while $X = 1$ corresponds to the downstream (rear) stagnation point where the flow detaches itself from the cylinder; see Fig. 1. We obtain

$$\theta'' + 2\eta\theta' = 2X\theta_X + \frac{H}{1-X^2}(\theta-\phi), \tag{11a}$$

$$\phi'' = \frac{H\gamma}{1-X^2}(\phi-\theta), \tag{11b}$$

where primes denote derivatives with respect to η. The boundary conditions which are required to complete the problem are that

$$\theta = \phi = 1 \quad \text{on } \eta = 0 \quad \text{and} \quad \theta, \phi \to 0 \quad \text{as } \eta \to \infty. \tag{12}$$

Eqs. (11) form a parabolic system even though (11b) does not contain single X-derivatives. The absence of such derivatives simply means that ϕ adjusts instantly to changes in θ as X increases, and may also be viewed as a differential constraint on the evolution of θ. Moreover this system is well-posed as (11a) reduces to an ordinary differential equation when $X = 0$. Therefore we have a pair of ODEs to solve at $X = 0$ and the solution of these provides the initial conditions for the subsequent evolution in X.

Numerical and asymptotic solutions of (11) are presented in subsequent sections in the form of both local and global rates of heat transfer. The local Nusselt numbers are given by

$$Nu_f = -\frac{\partial\theta}{\partial r}\bigg|_{r=1}, \qquad Nu_s = -\frac{\partial\phi}{\partial r}\bigg|_{r=1}, \tag{13}$$

and, in terms of η, these may be expressed more conveniently as

$$q_f = \frac{Nu_f}{Pe^{1/2}\sin\frac{1}{2}\alpha} = -\frac{\partial\theta}{\partial\eta}\bigg|_{\eta=0}, \qquad q_s = \frac{Nu_s}{Pe^{1/2}\sin\frac{1}{2}\alpha} = -\frac{\partial\phi}{\partial\eta}\bigg|_{\eta=0}. \tag{14}$$

The global rates of heat transfer, which are defined as the local values averaged between $\alpha = 0$ and $\alpha = \pi$, are then given by

$$Q_f = -\frac{1}{\pi}\int_0^{\pi} \frac{\partial\theta}{\partial\eta}\bigg|_{\eta=0} \sin\frac{1}{2}\alpha\,\mathrm{d}\alpha = -\frac{2}{\pi}\int_0^{1} \frac{\partial\theta}{\partial\eta}\bigg|_{\eta=0} \mathrm{d}X \tag{15a}$$

and

$$Q_s = -\frac{1}{\pi}\int_0^{\pi} \frac{\partial\phi}{\partial\eta}\bigg|_{\eta=0} \sin\frac{1}{2}\alpha\,\mathrm{d}\alpha = -\frac{2}{\pi}\int_0^{1} \frac{\partial\phi}{\partial\eta}\bigg|_{\eta=0} \mathrm{d}X. \tag{15b}$$

4. Numerical solutions

Eqs. (11) constitute a parabolic partial differential system which we solved numerically by the well-known Keller box method [22]. No substantial modification to a standard code is required except for the solution near $X = 1$. At this point we solve the equations

$$\theta'' + \frac{\gamma}{1+\gamma}2\eta\theta' = 0, \qquad \phi'' + \frac{\gamma}{1+\gamma}2\eta\phi' = 0 \tag{16a}$$

subject to $\theta = \phi = 1$ at $\eta = 0$ and $\theta, \phi \to 0$ as $\eta \to \infty$ since it is shown later that θ and ϕ are identical at $X = 1$ and satisfy these equations. In all cases the solutions evolve naturally to the solutions of Eqs. (16) which are

$$\theta = \phi = \mathrm{erfc}\left[\left(\frac{\gamma}{1+\gamma}\right)^{1/2}\eta\right]. \tag{16b}$$

During testing for accuracy it was found that the boundary layer thickness in terms of η varies very substantially with X, and the value of $\eta_{\max}$ chosen to obtain an accurate solution at $X = 0$ sometimes induced numerical convergence problems near $X = 1$ where the boundary layers can be much thinner in terms of η than is the boundary layer for the solid phase near $X = 0$. Therefore the solution was monitored as X varied and the value of $\eta_{\max}$ was chosen to be such that the computed value of ϕ' at $\eta = \eta_{\max}$ was held at approximately 10^{-6}. A more stringent criterion yields convergence difficulties, while a more relaxed condition affects adversely the accuracy of the solution. Apart from this additional facility, the Keller box code is as described in other published papers; see, for example, Rees [23,24] or Rees and Pop [16,17]. In all cases we used a constant steplength 0.05 in the η-direction. We also chose to use a constant steplength of 0.05 for X over most of the range $0 \leqslant X \leqslant 1$, but it was necessary to use decreasing steps on the approach to $X = 1$ since the solutions vary very rapidly when H and γ are small.

The computational results of the paper are summarised in Figs. 2 and 3 and in Tables 1 and 2. Fig. 2 shows how the local rates of heat transfer, q_f and q_s, vary with X and H for four different values of γ. In all cases common asymptotic values $(\gamma/(1+\gamma))^{1/2}(2/\sqrt{\pi})$ are achieved at $X = 1$, which corresponds to the rear stagnation point of the cylinder. The chief physical reason for this feature is that the boundary layer thickness in terms of $\hat{r}$ (see Eq. (10)) increases without limit as $X \to 1$, and this allows the two thermal fields to equilibrate to the same values.

As X increases from 0 towards 1 the local rate of heat transfer for the fluid decreases in magnitude, but that for the solid increases. Here, thermal diffusion effects for the solid phase are stronger relative to the fluid phase, and its thermal field spreads out to relatively greater distances because it is not affected directly by advection on the upstream side of the cylinder; the implication is that in all cases $q_s < q_f$. These phenomena are confirmed by the asymptotic analyses for both large and small values of H given in the next two sections.

A detailed study of the curves in Fig. 2 shows that large discrepancies between the rates of heat transfer of the fluid and the solid occur not only when H is relatively small, which is to be expected because this corresponds directly to cases where there is poor transfer of heat between the phases, but also when γ is small. (Fig. 2(a) in particular demonstrates this effect.) This may

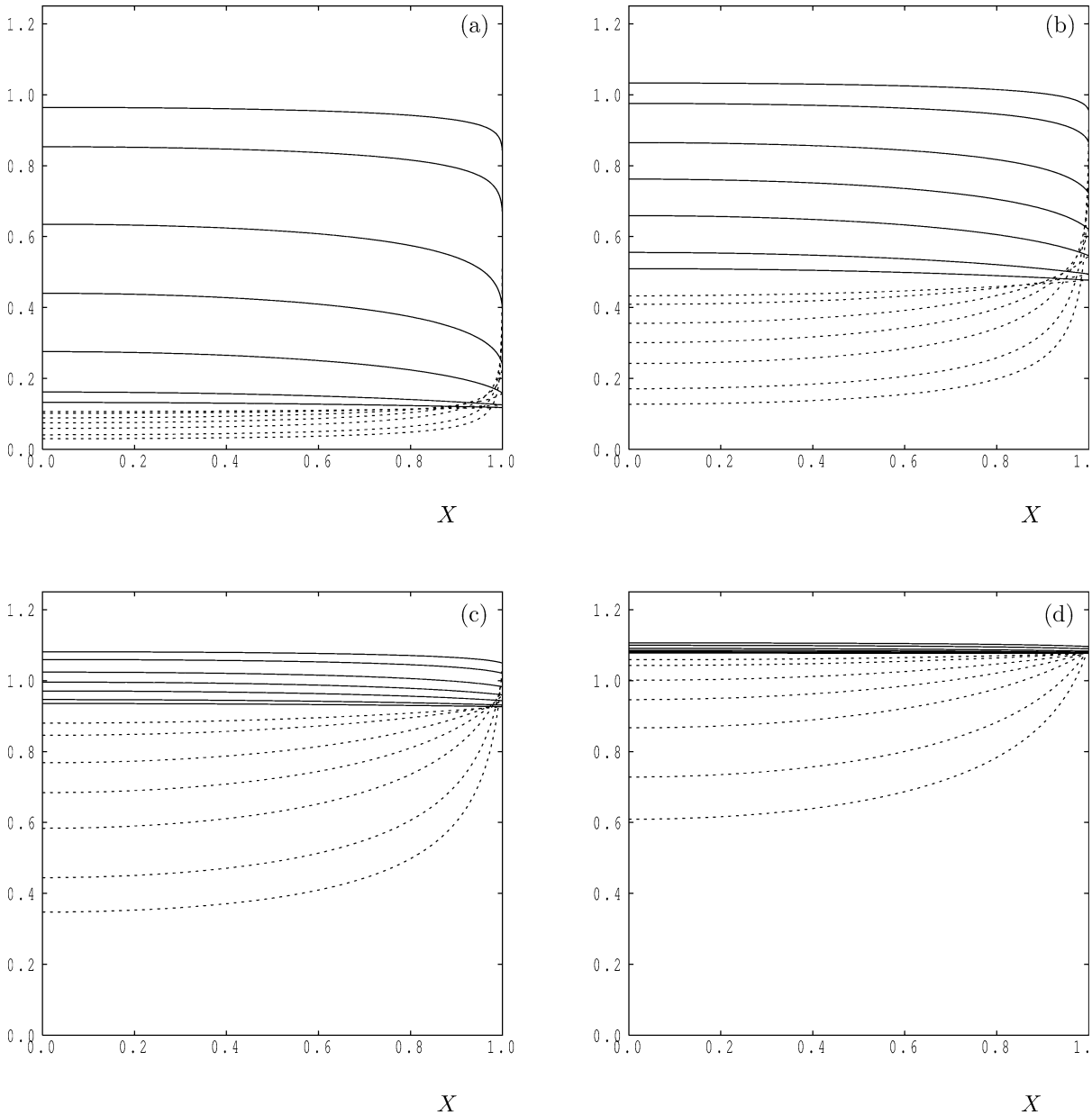

Fig. 2. Variation with X of the local rates of heat transfer around the cylinder. The continuous curves correspond to q_f and the dashed curves to q_s. Curves correspond to $H = 0.1$, 0.2, 0.5, 1.0, 2.0, 5.0 and 10.0; $H = 10$ corresponds to the lowest continuous curve and the highest dashed curve at $X = 0$ in each subfigure. (a) $\gamma = 0.1$; (b) $\gamma = 0.2$; (c) $\gamma = 2.0$; (d) $\gamma = 10.0$.

be explained by the fact that small values of γ correspond solely to the poor transfer of heat to or from the solid phase; in turn this enables the solid phase temperature field to be effectively independent of the fluid phase, thereby allowing heat to conduct outwards readily to give a correspondingly small magnitude of the rate of heat transfer. On the other hand, when γ is relatively large, such as is shown in Fig. 2(d), then the temperature field of the solid phase is affected very strongly by the temperature of the fluid phase. In Fig. 2(d) we see that, at such large values of γ, the temperature of the fluid phase is almost independent of both X and H. When H is small, then Eq. (11a) shows that the contribution to the fluid field from the solid is negligible since the only term coupling θ and ϕ is multiplied by H, whereas when H is large, then θ and ϕ are nearly identical. In both cases the term multiplying H in (11a) is small, and therefore the fluid temperature field is almost independent of X.

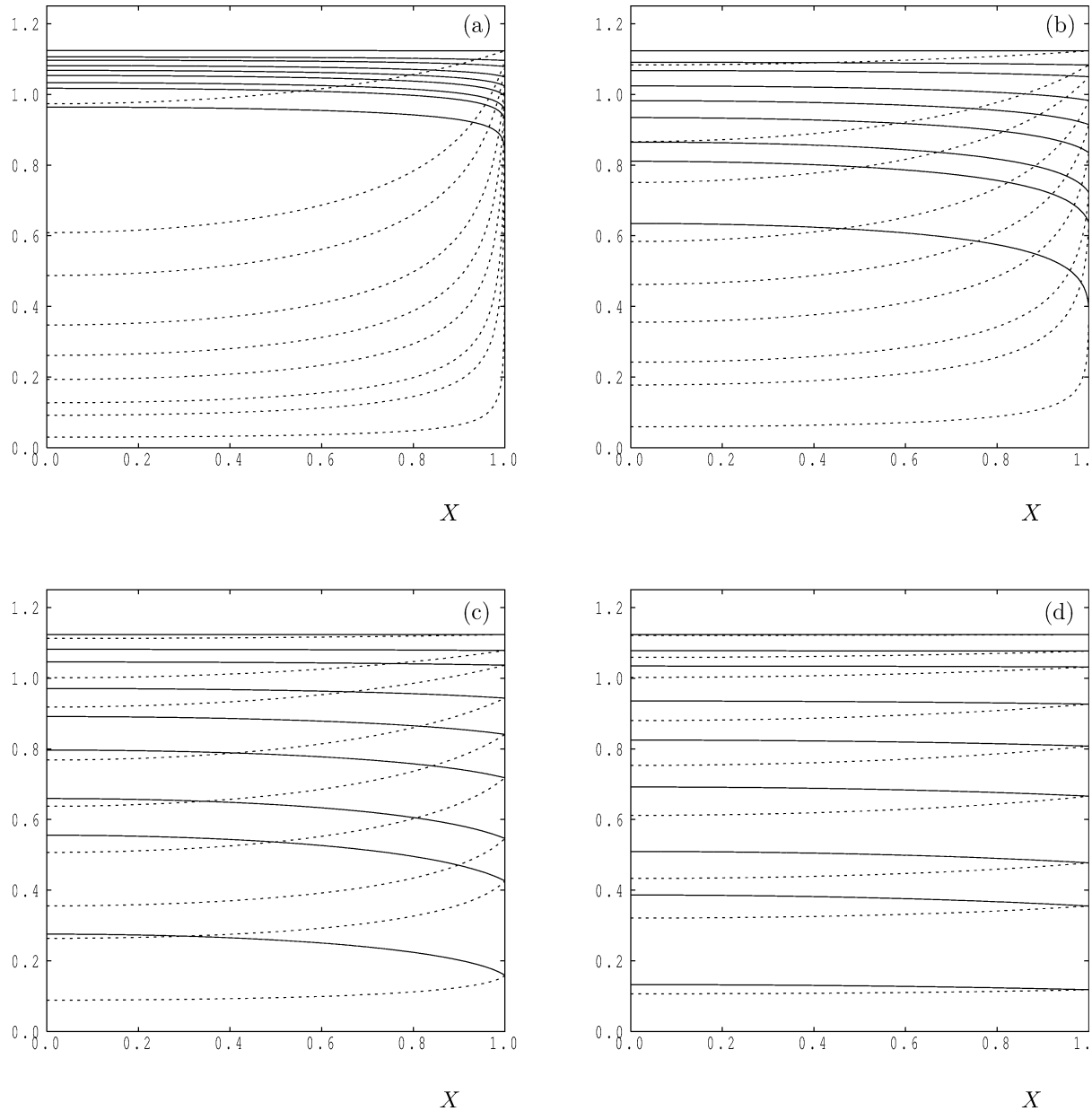

Fig. 3. Variation with X of the local rates of heat transfer around the cylinder. The continuous curves correspond to q_f and the dashed curves to q_s. Curves correspond to $\gamma = 0.01$, 0.1, 0.2, 0.5, 1.0, 2.0, 5.0, 10.0 and 100.0; $\gamma = 100$ corresponds to the highest pair of curves in each subfigure. (a) $H = 0.1$; (b) $H = 0.5$; (c) $H = 2.0$; (d) $H = 10.0$.

Fig. 3 presents an alternative view of the numerical results by illustrating the variation of q_f and q_s with X and γ for various chosen values of H. In general we see substantial differences between the q_f and q_s curves when either of the parameters H and γ are small. However, when H is large the values of q_f and q_s shown in Fig. 3(d) are quite close and both are almost independent of X. At the opposite extreme, represented by Fig. 3(a) for which $H = 0.1$, there is a very large difference between the heat transfer characteristics of the two phases. Once more this is due to near decoupling of Eq. (11a) from (11b). The decay of θ is superexponential, but ϕ decays like $\exp(-\eta\sqrt{H\gamma})$ when η is large. For small values of $H\gamma$ the slow decay of ϕ yields a small rate of heat transfer. However, when X increases, the value of $H\gamma/(1 - X^2)$ increases and thermal equilibrium is approached fairly quickly as $X \to 1$.

Table 1
Values of Q_f (defined by (15a)) as a function of γ and H

H	γ									
	0.01	0.1	0.2	0.5	1	2	5	10	100	1000
0.1	0.6055	0.6402	0.6509	0.6648	0.6750	0.6846	0.6958	0.7028	0.7156	0.7182
0.2	0.5293	0.5910	0.6102	0.6351	0.6530	0.6694	0.6877	0.6983	0.7153	0.7182
0.5	0.3825	0.4969	0.5339	0.5821	0.6159	0.6457	0.6766	0.6930	0.7152	0.7182
1.0	0.2571	0.4119	0.4657	0.5365	0.5858	0.6280	0.6695	0.6900	0.7151	0.7182
2.0	0.1580	0.3335	0.4017	0.4941	0.5587	0.6130	0.6641	0.6879	0.7150	0.7182
5.0	0.0961	0.2648	0.3421	0.4533	0.5331	0.5995	0.6597	0.6863	0.7150	0.7182
10.0	0.0815	0.2396	0.3179	0.4353	0.5216	0.5936	0.6579	0.6857	0.7150	0.7182

Table 2
Values of Q_s (defined by (15b)) as a function of γ and H

H	γ									
	0.01	0.1	0.2	0.5	1	2	5	10	100	1000
0.1	0.0281	0.0825	0.1121	0.1648	0.2165	0.2784	0.3728	0.4486	0.6472	0.7091
0.2	0.0371	0.1074	0.1448	0.2098	0.2712	0.3416	0.4421	0.5160	0.6761	0.7135
0.5	0.0500	0.1438	0.1923	0.2735	0.3461	0.4241	0.5241	0.5886	0.6978	0.7163
1.0	0.0587	0.1695	0.2261	0.3184	0.3976	0.4779	0.5724	0.6271	0.7060	0.7173
2.0	0.0648	0.1896	0.2532	0.3550	0.4389	0.5195	0.6067	0.6524	0.7104	0.7177
5.0	0.0689	0.2053	0.2756	0.3868	0.4750	0.5548	0.6335	0.6708	0.7131	0.7180
10.0	0.0702	0.2110	0.2843	0.4000	0.4903	0.5696	0.6441	0.6777	0.7141	0.7181

In the next two sections we examine in detail the temperature fields and their associated rates of heat transfer in the large-H and small-H limits.

5. Asymptotic solution for large values of H

Large values of H correspond to a high rate of heat transfer between the phases and it is to be expected that the fluid and solid thermal fields are very similar in this limit. It proves convenient to rewrite Eqs. (11) in terms of the variables θ and χ where

$$\chi = \phi - \theta, \tag{17}$$

is the temperature difference between the phases; we obtain

$$\left(1 + \frac{1}{\gamma}\right)\theta'' + 2\eta\theta' - 2X\theta_X = -\frac{1}{\gamma}\chi'' \tag{18}$$

and

$$\chi = \frac{1 - X^2}{H\gamma}(\chi'' + \theta''). \tag{19}$$

It is possible to make the leading order solution independent of γ by rescaling the independent variable, η, according to

$$\zeta = \left(\frac{\gamma}{1+\gamma}\right)^{1/2}\eta \tag{20}$$

and therefore we solve

$$\theta_{\zeta\zeta} + 2\zeta\theta_\zeta - 2X\theta_X = -\frac{1}{1+\gamma}\chi_{\zeta\zeta}, \tag{21}$$

and

$$\chi = \frac{1 - X^2}{H(1+\gamma)}(\chi_{\zeta\zeta} + \theta_{\zeta\zeta}). \tag{22}$$

The solution proceeds in terms of inverse powers of H: let

$$(\theta, \chi) = (\theta_0, \chi_0) + H^{-1}(\theta_1, \chi_1) + \cdots \tag{23}$$

and then at leading order we find that

$$\theta_0 = \operatorname{erfc}\zeta = \frac{2}{\sqrt{\pi}} \int_{\zeta}^{\infty} \mathrm{e}^{-s^2}\,\mathrm{d}s, \tag{24}$$

$$\chi_0 = 0, \tag{25}$$

while at $\mathrm{O}(H)$,

$$\theta_1 = \frac{4/\sqrt{\pi}}{(1+\gamma)^2}\left[\left(\frac{1}{2}\zeta^3 - \frac{3}{4}\zeta\right) + X^2\left(\frac{1}{2}\zeta - \frac{1}{3}\zeta^3\right)\right]\mathrm{e}^{-\zeta^2}, \tag{26}$$

$$\chi_1 = \frac{4/\sqrt{\pi}}{1+\gamma}(1-X^2)\zeta\,\mathrm{e}^{-\zeta^2}. \tag{27}$$

From these solutions we obtain

$$\left.\frac{\partial\theta}{\partial\zeta}\right|_{\zeta=0} = -\frac{2}{\sqrt{\pi}} + \frac{1}{\sqrt{\pi}(1+\gamma)^2}\left[-3+2X^2\right]H^{-1} + \cdots, \tag{28}$$

$$\left.\frac{\partial\phi}{\partial\zeta}\right|_{\zeta=0} = -\frac{2}{\sqrt{\pi}} + \frac{1}{\sqrt{\pi}(1+\gamma)^2}\left[(1+4\gamma) - (2+4\gamma)X^2\right]H^{-1} + \cdots. \tag{29}$$

We note that the $\mathrm{O}(H^{-1})$ contribution to the rate of heat transfer in the fluid phase is always less than that of the solid phase, except at the rear stagnation point, $X = 1$, at which point they are identical.

The local rates of heat transfer from the cylinder are given by

$$q_f \sim \left(\frac{\gamma}{1+\gamma}\right)^{1/2}\frac{2}{\sqrt{\pi}}\left[1 + \frac{1}{(1+\gamma)^2}\left(\frac{1}{2} + \sin^2\frac{1}{2}\alpha\right)H^{-1} + \cdots\right], \tag{30a}$$

$$q_s \sim \left(\frac{\gamma}{1+\gamma}\right)^{1/2}\frac{2}{\sqrt{\pi}}\left[1 + \frac{1}{(1+\gamma)^2}\left(\frac{1}{2} - (1+2\gamma)\sin^2\frac{1}{2}\alpha\right)H^{-1} + \cdots\right], \tag{30b}$$

and the corresponding global rates of heat transfer are

$$Q_f \sim \frac{4}{\pi^{3/2}}\left(\frac{\gamma}{1+\gamma}\right)^{1/2}\left[1 + \frac{7}{6(1+\gamma)^2}H^{-1}\right], \tag{31a}$$

$$Q_s \sim \frac{4}{\pi^{3/2}}\left(\frac{\gamma}{1+\gamma}\right)^{1/2}\left[1 - \frac{1+8\gamma}{6(1+\gamma)^2}H^{-1}\right]. \tag{31b}$$

We note that the leading terms in (30) and (31) yield the LTE results quoted by Pop and Yan [19] since the Péclet number used by those authors was based on the mean properties of the porous medium, rather than on the fluid properties.

Global rates of heat transfer for the fluid and solid phases as computed by the numerical routines described in Section 4 are listed in Tables 1 and 2 respectively. In all cases the value of Q_f is higher than Q_s. When H is large, the phases are very nearly in local thermal equilibrium and hence both rates are very close to the leading terms in (31a,b). Tables 3 and 4 show two comparisons between the numerical solutions obtained for $H = 100$ and the one and two-term asymptotic expressions given in (31). In both cases the addition of the second term in the asymptotic expansion yields an excellent agreement with the numerical simulations. Thus we may use (31) for larger values of H. However, we note that, as the value of γ reduces, so the quality of the agreement also reduces, although, at $\gamma = 0.01$, the relative error in Q_f is approximately 2×10^{-4}.

Table 3
Comparisons of the numerical values and the 1-term and 2-term large-H asymptotic representations of Q_f and Q_s for $\gamma = 0.01$

	Fluid	Solid
Numerical ($H = 100$)	7.2311×10^{-2}	7.1352×10^{-2}
1-term asymptotic	7.1478×10^{-2}	7.1478×10^{-2}
2-term asymptotic	7.2296×10^{-2}	7.1352×10^{-2}

Table 4
Comparisons of the numerical values and the 1-term and 2-term large-H asymptotic representations of Q_f and Q_s for $\gamma = 1$

	Fluid	Solid
Numerical ($H = 100$)	0.50943	0.50608
1-term asymptotic	0.50795	0.50795
2-term asymptotic	0.50943	0.50604

6. Asymptotic solution for small values of H

Now we look at the opposite asymptotic extreme $H \ll 1$ which relates to the case when there is relatively poor heat transfer between the phases. A straightforward perturbation expansion in powers of H fails at leading order since the equation for ϕ ($\phi'' = 0$; see Eq. (11b)) cannot be solved subject to both boundary conditions specified in (12). Previous experience suggests that this indicates the presence of a very thick outer region, and this is confirmed by the numerical work. Once more, a standard analysis involving a power series in $H^{1/2}$ and the method of matched asymptotic expansions is inappropriate since the inner $O(H)$ equation for θ yields a solution which grows logarithmically as η increases. The resolution of this difficulty, which was absent in previous analyses where LTE is not present (see Rees and Pop [16] and [17]), involves an expansion of the type

$$(\theta, \phi) = (\theta_0, \phi_0) + H^{1/2}(\theta_1, \phi_1) + H \ln H\,(\theta_{2L}, \phi_{2L}) + H\,(\theta_2, \phi_2) + H^{3/2}(\theta_3, \phi_3) + \cdots \tag{32}$$

when $\eta = O(1)$. The outer region may easily be shown to have thickness, $H^{-1/2}$, and it may be studied using

$$(\theta, \phi) = (\Theta_0, \Phi_0) + H^{1/2}(\Theta_1, \Phi_1) + H(\Theta_2, \Phi_2) + H^{3/2}(\Theta_3, \Phi_3) + \cdots, \tag{33}$$

where $\eta \equiv H^{-1/2}Y$ and the Θ_j and Φ_j are all functions of Y. Expansions (32), (33) when substituted into system (11) leads to a hierarchy of equations for the coefficient functions which may be solved order by order. The zeroth order inner problem gives

$$\theta_0 = \operatorname{erfc}(\eta) = \frac{2}{\sqrt{\pi}} \int_{\eta}^{\infty} \mathrm{e}^{-s^2}\,\mathrm{d}s, \qquad \phi_0 = 1 \tag{34}$$

and the form of ϕ_0 is consistent with the fact that the numerical solutions decay very slowly for the solid phase, and it is this which motivates the use of an outer region. Now also

$$\Theta_0 = 0, \qquad \Phi_0 = \exp\left[-\frac{\sqrt{\gamma}}{\sqrt{1 - X^2}} Y\right] \tag{35}$$

so that the solution for Φ_0 decays to zero as $Y \to \infty$, which is as expected from a physical point of view. The solution for the fluid phase shows that there is no leading order thermal penetration into the outer region. Clearly the solution for Φ_0 breaks down in the limit as $X \to 1$, and therefore the following solutions are valid only when $1 - X = O(1)$.

The $O(H^{1/2})$ parts of (32), (33) are easily evaluated as

$$\theta_1 = 0, \qquad \phi_1 = -\left(\frac{\gamma}{1 - X^2}\right)^{1/2} \eta, \qquad \Theta_1 = \Phi_1 \equiv 0 \tag{36}$$

while the terms of size $O(H \ln H)$ lead to

$$\theta_{2L} = C_1 \int_0^{\eta} \mathrm{e}^{-s^2}\,\mathrm{d}x, \qquad \phi_{2L} = 0, \tag{37}$$

for some constant C_1. With this, the equation for θ_2 becomes

$$\theta_2'' + 2\eta\theta_2' - 2X\theta_{2X} = -\frac{2/\sqrt{\pi}}{1 - X^2} \int_0^{\eta} \mathrm{e}^{-s^2}\,\mathrm{d}s \equiv \frac{A(\eta)}{1 - X^2}, \tag{38}$$

which defines $A(\eta)$ as a multiple of the error function, and then

$$\theta_2 = B_0(\eta) + \frac{1}{4} A(\eta) \ln\bigl(1 - X^2\bigr), \tag{39}$$

where

$$B_0'' + 2\eta B_0' = -\frac{2}{\sqrt{\pi}} \int_0^\eta \mathrm{e}^{-s^2}\,\mathrm{d}s = -\operatorname{erf}(\eta). \tag{40}$$

This equation cannot easily be solved analytically but $B_0 \sim -\frac{1}{2}\ln\eta + C_2$ as $\eta \to \infty$ where C_2 is a constant which may be obtained numerically using an outer region solution; at this stage it cannot be tied down. The corresponding large-η behaviour of θ_2 is

$$\theta_2 \sim \left[-\frac{1}{2}\ln\eta + C_2\right] - \frac{1}{4}\ln\bigl(1 - X^2\bigr), \tag{41}$$

while ϕ_2 may be found explicitly

$$\phi_2 = \frac{\gamma}{2\sqrt{\pi}(1-X^2)}\left[\eta\,\mathrm{e}^{-\eta^2} + \bigl(2\eta^2+1\bigr)\int_0^\eta \mathrm{e}^{-s^2}\,\mathrm{d}s\right]. \tag{42}$$

It turns out that we do not have to consider the outer $\mathrm{O}(H)$ equations before solving the inner solutions at $\mathrm{O}(H^{3/2})$. It follows that

$$\theta_3 = C_3\int_0^\eta \mathrm{e}^{-s^2}\,\mathrm{d}s + \frac{\sqrt{\gamma}(1-2X^2)}{2\sqrt{1-X^2}}\eta, \qquad \phi_3 = -\frac{1}{6}\left(\frac{\gamma}{1-X^2}\right)^{3/2}\eta^3 + C_4\eta, \tag{43,44}$$

where C_3 and C_4 are constants.

6.1. Asymptotic matching

For large values of η the inner solutions re-expressed in terms of the outer variable $Y = H^{1/2}\eta$ are

$$\theta \sim H\ln H\left[\frac{1}{4} + \frac{1}{2}\sqrt{\pi}C_1\right] + H\left[-\frac{1}{2}\ln Y + C_2 - \frac{1}{4}\ln\bigl(1-X^2\bigr) + \frac{\sqrt{\gamma}(1-2X^2)Y}{2\sqrt{1-X^2}}\right] + H^{3/2}\left[\frac{1}{2}\sqrt{\pi}C_3\right] \tag{45}$$

and

$$\phi \sim \left[1 - \left(\frac{\gamma}{1-X^2}\right)^{1/2}Y + \frac{1}{2}\left(\frac{\gamma}{1-X^2}\right)Y^2 - \frac{1}{6}\left(\frac{\gamma}{1-X^2}\right)^{3/2}Y^3 + \cdots\right] + H\left[\frac{\gamma}{4(1-X^2)} + C_4 Y\right]. \tag{46}$$

Now the term involving $H\ln H$ in expansion (45) may be removed by setting $C_1 = -1/(2\sqrt{\pi})$ which precludes the need for terms of $\mathrm{O}(H\ln H)$ in the outer region.

We are now in a position to be able to solve the $\mathrm{O}(H)$ outer problem using (45) and (46) to inform us of the requisite $Y \to 0$ matching conditions.

6.2. Outer solutions at $\mathrm{O}(H)$

We already have expressions for Θ_0, Θ_1, Φ_0 and Φ_1; see Eqs. (36). At $\mathrm{O}(H)$ the equation for Θ_2 is

$$2Y\Theta_2' - 2X\Theta_{2X} = -\frac{1}{1-X^2}\exp\left[-\left(\frac{\gamma}{1-X^2}\right)^{1/2}Y\right] \tag{47}$$

but it is not necessary to solve this as it is possible to develop an expansion for small values of Y. The result is that

$$\Theta_2 = -\frac{1}{2}\ln Y + \left[-\frac{1}{4}\ln\bigl(1-X^2\bigr) + C_2\right] + \frac{1}{2}\sqrt{\gamma}\frac{(1-2X^2)}{\sqrt{1-X^2}}Y + \cdots \tag{48}$$

for $Y \ll 1$ and the Y-independent term clearly has its counterpart in Eq. (45).

Table 5
Comparisons of the numerical values and the 1-term and 2-term small-H asymptotic representations of Q_f and Q_s for $\gamma = 1$

	Fluid	Solid
Numerical ($H = 10^{-3}$)	0.71715	0.029849
1-term asymptotic	0.71835	0.031623
2-term asymptotic	0.71711	

6.3. Rates of heat transfer

We may now find the local and global rates of heat transfer for both phases using the above solutions in the inner region. The local rates of heat transfer are given by

$$q_f = \frac{2}{\sqrt{\pi}} + \frac{1}{2\sqrt{\pi}} H \ln H + \mathrm{O}(H), \tag{49}$$

$$q_s = \sqrt{\frac{\gamma}{1-X^2}} H^{1/2} - \frac{\gamma}{\sqrt{\pi}(1-X^2)} H + \mathrm{O}\big(H^{3/2}\big) \tag{50}$$

for small values of H. The small magnitude of the leading term in (50) reflects the fact that the solid phase boundary layer is much thicker than that of the fluid phase.

These expressions may now be integrated according to Eqs. (15) to obtain the global rates of heat transfer. This may be done for the fluid phase, but for the solid phase the expressions for the local rate of heat transfer are not uniformly valid. Therefore the most that may be claimed is that

$$Q_f = \frac{4}{\pi^{3/2}} + \frac{H \ln H}{\pi^{3/2}} + \mathrm{O}(H) \quad \text{and} \quad Q_s = \gamma^{1/2} H^{1/2} + \mathrm{o}\big(H^{1/2}\big). \tag{51}$$

Strictly speaking it is necessary to examine in detail how the thermal field is modified in the region close to $X = 1$. The critical region is when $X = 1 - \mathrm{O}(H)$, but we do not pursue such a study in the present paper.

Table 5 shows a comparison between the computed values of Q_f and Q_s and the asymptotic values given by (51). The addition of the second term for Q_f reduces the relative error from being just less than 2×10^{-3} to one which is of magnitude 1×10^{-5}. The one-term approximation for Q_s is not as good but has relative error 6×10^{-2}. It is expected that these correlations improve for smaller values of γ, but require yet smaller values of H to maintain the present accuracy when larger values of γ are taken.

7. Conclusions

In this paper we have examined the steady forced convection boundary layer flow past a hot circular cylinder which is embedded in a fluid-saturated porous medium where a two-temperature model of the microscopic heat transfer between the solid and fluid phases has been adopted. The heat transfer coefficients for the fluid and solid phases have been computed numerically by solving the appropriate parabolic partial differential equations. Detailed asymptotic analyses for both large and small values of H have been undertaken, the latter using the method of matched asymptotic expansions.

When the porous medium is in thermal equilibrium the local heat transfer coefficients defined in (14) do not vary with α. In general, when local thermal nonequilibrium applies the developing thermal field in each phase is nonsimilar, and the local heat transfer coefficients vary with α. It was found that as the angle, α, decreases from $\alpha = \pi/2$ (i.e., the front stagnation point or $X = 0$) to $\alpha = 0$ (the rear stagnation point or $X = 1$), the local rate of heat transfer for the fluid phase decreases in magnitude, but that for the solid phase increases and in all circumstances $Q_s < Q_f$. Near the leading stagnation point the rate of heat transfer in the fluid phase is relatively high as this is where advection of cold fluid towards the cylinder occurs. The solid phase is immune to these effects, when H is not large, and therefore heat is able to conduct more readily away from the cylinder, which, in turn, reduces its rate of heat transfer relative to the fluid phase. Towards the rear stagnation point, on the other hand, the boundary layer has become much thicker, and the temperature fields are able to equilibriate.

When either H or γ are sufficiently small, then the temperature field of the fluid phase, which is dominated by a balance between conduction and advection, has little influence on the evolution of temperature field of the solid phase. The latter grows quite substantially as H or γ decrease towards zero, and this reduces both the local and global rates of heat transfer very markedly. In all cases, however, thermal equilibrium is established towards the rear of the cylinder.

Finally we make a comment on the realisability of the flows described here. We have computed a steady flow where heat is being lost from a hot cylinder to a cold fluid stream. At some point on the cylinder, the location of which is dependent of the direction of the gravity vector, there will be a situation where hot fluid underlies cold fluid and there exists the possibility of thermal instability due to an unstable temperature gradient. However it is very unlikely that instability should arise in the present flow because the local Darcy–Rayleigh number (which must be above $4\pi^2$ for instability to exist in the Darcy–Bénard problem) is proportional to the thickness of the region over which the temperature variation takes place. For the forced convection flow considered here, the Pèclet number is large, and therefore the boundary layer thickness is very small. In turn, the Darcy–Rayleigh number is also small, and therefore the flow will be stable. Such an occurrence may not exist when the Péclet number is finite.

Acknowledgements

Much of this investigation was performed while APB was on study leave at the University of New South Wales. He is indebted to the Royal Society of London and the Australian Research Council without whose grants his visit would not have been possible. In addition, he is grateful to the staff and students of New College UNSW, Dr. Peter Blennerhassett and the School of Mathematics for their hospitality. IP also wishes to thank the Royal Society of London for partial support while he visited the University of Leeds, UK.

References

[1] D.B. Ingham, I. Pop (Eds.), Transport Phenomena in Porous Media, Vol. II, Pergamon, Oxford, 1998, 2002.
[2] D.A. Nield, A. Bejan, Convection in Porous Media, 2nd edition, Springer, New York, 1999.
[3] K. Vafai, Handbook of Porous Media, Marcel Dekker, New York, 2000.
[4] D.A. Nield, A.V. Kuznetsov, Local thermal nonequilibrium effects in forced convection in a porous medium channel: a conjugate problem, Int. J. Heat Mass Transfer 42 (1999) 3245–3252.
[5] D.A. Nield, A.V. Kuznetsov, M. Xiong, Effect of local thermal nonequilibrium on thermally developing forced convection in a porous medium, Int. J. Heat Mass Transfer 45 (2002) 4949–4955.
[6] M. Combarnous, Description du transfert de chaleur par convection naturelle dans une couche poreuse horizontale a l'aide d'un coefficient de transfert solide–fluide, C. R. Acad. Sci. Paris, Ser. A 275 (1972) 1375–1378.
[7] M. Combarnous, S. Bories, Modelisation de la convection naturelle au sein d'une couche poreuse horizontal a l'aide d'un coefficient de transfert solide–fluide, Int. J. Heat Mass Transfer 17 (1974) 505–515.
[8] M. Sözen, K. Vafai, Analysis of the non-thermal equilibrium condensing flow of a gas through a packed bed, Int. J. Heat Mass Transfer 33 (1990) 1247–1261.
[9] M. Sözen, K. Vafai, L.A. Kennedy, Thermal charging and discharging of sensible and latent heat storage packed beds, J. Thermophys. Heat Transfer 5 (1991) 1247–1261.
[10] A. Amiri, K. Vafai, Analysis of dispersion effects and non-thermal equilibrium, non-Darcian, variable porosity incompressible flow through porous media, Int. J. Heat Mass Transfer 37 (1994) 939–954.
[11] A.V. Kuznetsov, A perturbation solution for a nonthermal equilibrium fluid flow through a three-dimensional sensible heat storage packed bed, Trans. ASME J. Heat Transfer 118 (1996) 508–510.
[12] A.V. Kuznetsov, Investigation of a non-thermal equilibrium flow of an incompressible fluid in a cylindrical tube filled with porous media, J. Appl. Math. Phys. (ZAMP) 76 (1996) 411–418.
[13] A.V. Kuznetsov, Analysis of a non-thermal equilibrium fluid flow in a concentric tube annulus filled with a porous medium, Int. Comm. Heat Mass Transfer 23 (1996) 929–938.
[14] A.V. Kuznetsov, Thermal nonequilibrium forced convection in porous media, in: D.B. Ingham, I. Pop (Eds.), Transport Phenomena in Porous Media, Pergamon, Oxford, 1998, pp. 103–129.
[15] K. Vafai, A. Amiri, Non-Darcian effects in combined forced convective flows, in: D.B. Ingham, I. Pop (Eds.), Transport Phenomena in Porous Media, Pergamon, Oxford, 1998, pp. 313–329.
[16] D.A.S. Rees, I. Pop, Free convection stagnation-point flow in a porous medium using a thermal nonequilibrium model, Int. Comm. Heat Mass Transfer 26 (1999) 945–954.
[17] D.A.S. Rees, I. Pop, Vertical free convection boundary layer flow in a porous medium using a thermal nonequilibrium model, J. Porous Media 3 (2000) 31–44.
[18] D.A.S. Rees, Vertical free convection boundary-layer flow in a porous medium using a thermal nonequilibrium model: elliptic effects, Z. Math. Phys. 54 (2003) 437–448.
[19] I. Pop, B. Yan, Forced convection flow past a cylinder and a sphere in a Darcian fluid at large Péclet numbers, Int. Comm. Heat Mass Transfer 25 (1998) 261–267.
[20] T. Sano, Unsteady heat transfer from a circular cylinder immersed in a Darcy flow, J. Engrg. Math. 14 (1980) 177–190.
[21] S. Wong, D.A.S. Rees, I. Pop, Forced convection past a heated horizontal cylinder in a porous medium using a thermal nonequilibrium model: finite Péclet number effects, Int. J. Thermal Sci., 2003, in press.

[22] T. Cebeci, P. Bradshaw, Physical and Computational Aspects of Convective Heat Transfer, Springer, New York, 1984.
[23] D.A.S. Rees, Three-dimensional free convection boundary layers in porous media induced by a heated surface with spanwise temperature variations, Trans. ASME J. Heat Transfer 119 (1997) 792–798.
[24] D.A.S. Rees, Free convective boundary layer flow from a heated surface in a layered porous medium, J. Porous Media 2 (1999) 39–58.